Multiobjective Co-Optimization of Cooperative Adaptive Cruise Control and Energy Management Strategy for PHEVs

Yinglong He, Quan Zhou, Michail Makridis, Konstantinos Mattas, Ji Li, Huw Williams, and Hongming Xu

***Abstract*— Electrification, automation, and connectivity in the automotive and transport industries are gathering momentum, but there are escalating concerns over their need for co-optimization to improve energy efficiency, traffic safety, and ride comfort. Previous approaches to these multiobjective co-optimization problems often overlook tradeoffs and scale differences between the objectives, resulting in misleading optimizations. To overcome these limitations, this article proposes a Pareto-based framework that demonstrably optimizes the system parameters of the cooperative adaptive cruise control (CACC) and the energy management strategy (EMS) for plug-in hybrid electric vehicles (PHEVs). The high-level Pareto knowledge assists in finding a best compromise solution. The results of this article suggest that the energy and the comfort targets are harmonious, but both conflict with the safety target. Validation using real-world driving data shows that the Pareto optimum for CACC and EMS systems, relative to the baseline, can reduce energy consumption (by 7.57%) and tracking error (by 68.94%) while simultaneously satisfying ride comfort needs. In contrast to the weighted-sum method, the proposed Pareto method can optimally balance and scale the multiple-objective functions. In addition, sensitivity analysis proves that the vehicle reaction time impacts significantly on tracking safety, but its effect on energy saving is trivial.**

***Index Terms*— Cooperative adaptive cruise control (CACC), energy consumption, energy management strategy (EMS), multiobjective co-optimization, tracking safety.**

I. Introduction

ENERGY, environmental, and safety challenges are exacerbated by rising transport demand [1]. To tackle these problems, vehicle electrification, automation, and connectivity are gathering momentum worldwide [2]–[4], but there are escalating concerns over their synergistic impacts on the control design of vehicles that fuse mechatronics with new informatics, such as plug-in hybrid electric vehicles (PHEVs) with automated driving systems.

Manuscript received October 17, 2019; revised December 23, 2019 and January 29, 2020; accepted February 3, 2020. Date of publication February 17, 2020; date of current version March 20, 2020. This work was supported in part by the Innovate UK under Grant 102253 and in part by the State Key Laboratory of Automotive Safety and Energy, Tsinghua University under Project KF2029. *(Corresponding author: Hongming Xu.)*

Yinglong He, Quan Zhou, Ji Li, Huw Williams, and Hongming Xu are with the Department of Mechanical Engineering, University of Birmingham, Birmingham, B15 2TT, U.K. (e-mail: yxh701@bham.ac.uk; q.zhou@bham.ac.uk; h.williams.5@bham.ac.uk; h.m.xu@bham.ac.uk).

Michail Makridis and Konstantinos Mattas are with the Directorate for Energy, Transport and Climate Change, European Commission–Joint Research Centre (JRC), 21027 Ispra, Italy (e-mail: michail.makridis@ec.europa.eu; konstantinos.mattas@ext.ec.europa.eu).

Digital Object Identifier 10.1109/TTE.2020.2974588

PHEVs are widely promoted as an efficient and clean solution that combines an internal combustion engine (ICE) with an electric motor and a large rechargeable battery. This hybrid powertrain enables all-electric driving for extended periods of time and overcomes the concern of range anxiety [5], [6]. Intensive efforts on PHEVs have developed energy management strategies (EMSs) for coordinating the power split in a fuel-efficient way [7]. However, the performance of EMS is often compromised by the complexity and uncertainty of driving conditions. It is, therefore, desirable to synergize internal powertrain coordination and external driving behavior [8]. Meanwhile, the longitudinal driving task gradually shifts from the human driver to in-vehicle automated systems. For example, the radar-aided adaptive cruise control (ACC) and the communication-enabled cooperative ACC (CACC) can regulate the vehicle speed to maintain a user-specified time headway or reach the user-desired speed [9]–[11]. These automated driving systems are designed to improve energy efficiency, road safety, and traffic throughput by optimizing velocity trajectories (i.e., ecodriving), which can be integrated with the EMS to further boost fuel economy [12]. Consequently, the co-optimization of CACC/ACC and EMS is gaining traction among automakers and policymakers [13].

Vehicles operate in the three longitudinal driving modes of free flow, car following, and platooning. Accordingly, studies on CACC/ACC and EMS co-optimization can be divided into the following three groups [14].

1) Studies for free-flow scenarios [15]–[17] usually deal with road constraints, such as speed limits, traffic lights, and road intersections. For example, a powertrain and speed integrated control was proposed to achieve 5.0%–16.9% fuel economy benefits, by utilizing the road topography and the dynamic speed limit [18]. Predictive energy optimization for connected and automated PHEVs was reported to deliver a fuel saving of 10.1% when considering the benefits of traffic light phasing [19].
2) Studies for car-following scenarios [20]–[22] mainly address the constraints of the movement of the preceding vehicle, to improve fuel economy, tracking safety, and so on. For instance, a predictive car-following power management system for PHEVs was demonstrated to simultaneously coordinate battery state-of-charge (SoC) planning, intervehicle spacing, and power split in a cost-optimal manner [23]. By adopting similar techniques,

a deep fusion method with ACC and EMS claimed to reduce fuel consumption by 5% [24].

3) Studies for platooning scenarios [25], [26] are primarily concerned with interactions between multiple vehicles. In a study on integrated optimization of internal powertrain energy management and external driving coordination for multiple hybrid electric vehicles (HEVs), the optimal results indicated a fuel saving of 17.9% compared with their baseline counterparts [27]. A two-layer hierarchical control system was constructed for a set of connected HEVs on a hilly terrain [28]. The top layer was tasked with cooperative driving and battery SoC planning; the bottom layer determined the power split and the gear shifting strategy.

From the perspective of objective functions, prior studies on CACC/ACC and EMS co-optimization problems are classified into the following two types.

1) Some studies investigate single-objective co-optimization [29], [30], which generally minimizes fuel consumption by optimizing speed trajectory and power split. However, this can only satisfy the fuel economy needs, neglecting comprehensive vehicle performance improvements.
2) Other studies highlight multiobjective co-optimization [22]–[24], addressing various needs including energy efficiency, tracking safety, ride comfort, and traffic throughput, especially in car-following and platooning scenarios. Previous studies converted the original CACC/ACC and EMS co-optimization with multiple objectives into a single-objective optimization problem by weighted-sum methods. For example, in a nonlinear model predictive control (NMPC) system, the safety and the energy targets are integrated into a cost function using a 2-D weight vector [21].

The weighted-sum methods cannot, however, determine the weights and the normalization factors that can optimally balance and scale the multiple-objective functions for a problem with little or no information [31], which can cause misleading optimization results. For example, in a study on multiobjective ACC and EMS co-optimization [32], the weighted-sum method led to an overoptimized fuel economy (a fuel saving of 7.07%), which in turn compromised other attributes such as tracking safety (an increase in tracking error of 10.5%).

To overcome these limitations, we propose a Pareto-based framework dealing with the multiobjective CACC and EMS co-optimization for PHEVs. The high-level knowledge (e.g., tradeoffs and scale differences between the objectives) of the Pareto frontier (PF) assists in finding a best compromise solution. The results of this study suggest that the energy and the comfort targets are harmonious, but both conflict with the safety target. These objective values are measured on different scales. In the validation using real-world driving data, the Pareto optimum for CACC and EMS systems, compared with the baseline scheme, can reduce energy consumption (by 7.57%) and tracking error (by 68.94%) while simultaneously satisfying ride comfort needs. In contrast to the weighted-sum method, the Pareto method can optimally balance and scale the multiple-objective functions and thus accurately capture the decision maker's preferences. In addition, sensitivity analysis proves that the vehicle reaction time impacts significantly on tracking safety, but its effect on energy saving is trivial.

The rest of this article is structured as follows. Section II describes the integrated CACC and EMS control framework as well as the augmented system dynamics for car following and power split. Section III presents the multiobjective problem and optimization methods. In Section IV, optimization results from the Pareto and the weighted-sum methods are compared. Section V concludes this article by summarizing the main findings.

II. Augmented System Dynamics and Integrated Control Framework

Fig. 1 shows the integrated CACC and EMS control framework as well as the augmented system dynamics for car following and power split. Their mathematical models are elaborated in the following.

A. Longitudinal Driving Dynamics

The longitudinal motion dynamics of the following vehicle are described by the equations:

$$\begin{cases} v_f = \dot{x_f} \\ a_f = \dot{v_f} \\ m_0 a_f = \dfrac{1}{r} T_d - \dfrac{1}{2}\rho C_d A_f v_f^2 - f m_0 g \cos\theta \\ \qquad\qquad - m_0 g \sin\theta, \end{cases} \tag{1}$$

where x_f, v_f, and a_f denote the longitudinal position (m), velocity (m/s), and acceleration (m/s^2), respectively; r is the wheel radius (m); T_d represents the driving torque (N·m) on the wheel axle; m_0 is the vehicle operating mass (kg); ρ is the air density (kg/m^3); C_d stands for the air drag coefficient; A_f is the vehicle effective frontal area (m^2); θ is the road slope (rad); g is the gravitational constant (9.8 m/s^2); and f is the rolling resistance coefficient.

B. Cooperative Adaptive Cruise Control

According to the CACC systems reported in previous studies [33], [34], the acceleration demand a_f can be computed based on the intervehicle spacing and the relative speed a_f^n or on the difference between the actual speed and the maximum safe speed a_f^m. Consequently, the following vehicle adopts the more restrictive choice as follows:

$$\begin{cases} a_f(t) = \min\left(a_f^n(t), a_f^m(t)\right) \\ a_f^n(t) = a_l(t-\tau) + k_v\left(v_l(t-\tau) - v_f(t-\tau)\right) \\ \qquad\qquad + k_s(s(t-\tau) - s_{\text{des}}) \\ a_f^m(t) = \left(v_f^{\max} - v_f(t)\right)/t_s \end{cases} \tag{2}$$

where a_l and v_l are the leading vehicle's acceleration (m/s^2) and speed (m/s), respectively. τ denotes the reaction time (s), including communication, sensing, and actuation delays. Here, t_s represents the control sample time (0.1 s), s is the bumper-to-bumper spacing (m), s_{des} is the desired intervehicle spacing (m), $v_f^{\max}$ is the maximum safe speed (m/s), and k_v

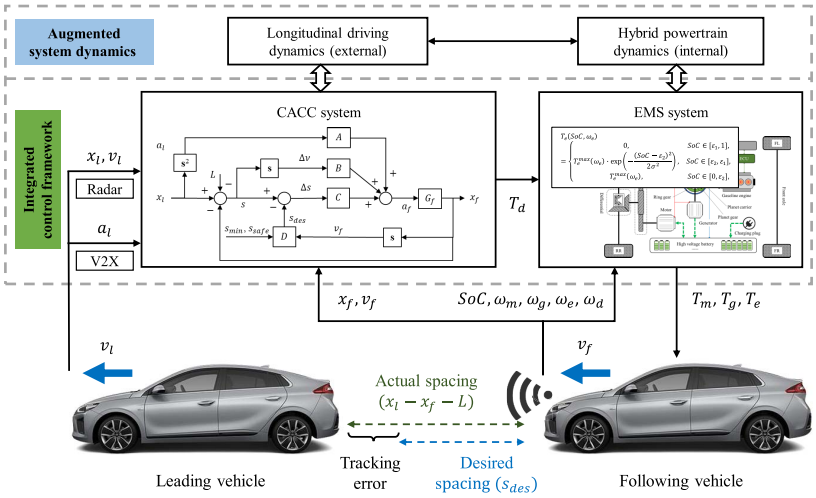

Fig. 1. Augmented system dynamics and the integrated control framework.

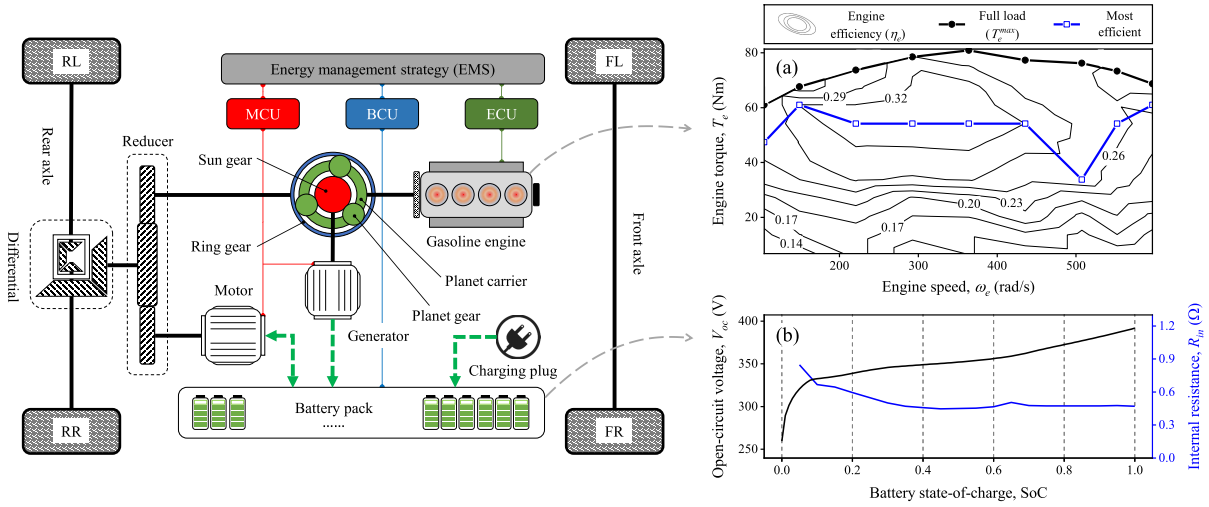

Fig. 2. Power-split PHEV powertrain (left) and the dynamics of (a) engine and (b) battery pack.

and k_s are the gain factors to minimize the speed difference and the tracking error, respectively.

The desired spacing s_{des} is the maximum among the following distance s_{hw} according to the time headway setting, the safe following distance s_{safe} considering the deceleration capabilities of the vehicles, and the minimum allowed distance s_{min} as described by:

$$\begin{cases} s_{\text{des}} = \max(s_{\text{hw}}, s_{\text{safe}}, s_{\text{min}}) \\ s_{\text{hw}} = v_f t_{\text{hw}} \\ s_{\text{safe}} = \dfrac{v_f^2}{2}\left(\dfrac{1}{b_f^{\max}} - \dfrac{1}{b_l^{\max}}\right) \end{cases} \tag{3}$$

where s_{min} is the minimum clearance (2.0 m) in the standstill situation, t_{hw} is the system-specified time headway (s), and $b_l^{\max}$ and $b_f^{\max}$ are negative numbers indicating the maximum braking decelerations (m/s^2) of the leader and the follower, respectively.

The maximum safe speed $v_f^{\max}$ is an important constraint for avoiding rear-end collisions when the leading vehicle initiates emergency braking, which can be expressed as

$$\begin{cases} v_f^{\max} = \sqrt{-2b_f^{\max} s_0} \\ s_0 = (x_l - x_f - L) - v_f \tau - \dfrac{v_l^2}{2b_l^{\max}} \end{cases} \tag{4}$$

where x_l and L are the leading vehicle's position and exterior length, respectively.

C. Hybrid Powertrain Dynamics

Fig. 2 (left) shows the PHEV powertrain with a power-split configuration [27]. This system divides the engine power along the two paths through a mechanical gear set; one path goes to the generator to produce electricity, while the other one drives the wheels.

The planetary gear assembly consists of a planet carrier, a sun gear, and a ring gear that are connected to the gasoline engine, the generator, and the reducer, respectively. Their

torque balance is given by

$$\begin{cases} T_m = -\left(\dfrac{r_r}{r_s + r_r}\right) T_e + \dfrac{1}{\kappa_c} T_d \\ \omega_m = \kappa_c \omega_d \\ T_g = -\left(\dfrac{r_r}{r_s + r_r}\right) T_e \\ \omega_e = \left(\dfrac{r_r}{r_s + r_r}\right) \omega_m + \left(\dfrac{r_s}{r_s + r_r}\right) \omega_g, \end{cases} \tag{5}$$

where T_e, T_m, and T_g indicate torques (N·m) that are, respectively, delivered from the engine, the motor, and the generator; ω_e, ω_m, ω_g, and ω_d are, respectively, the angular velocities (rad/s) of the engine, the motor, the generator, and the driveline; κ_c is the fixed gear ratio of the reducer; and r_s and r_r are, respectively, the radii of the sun gear and the ring gear.

The 1.5-L gasoline engine is modeled using its empirical performance map, as shown in Fig. 2(a). According to the data in the map, the instantaneous fuel consumption rate $\dot{m}_f$ (g/s) is calculated by

$$\dot{m}_f = \frac{T_e \omega_e}{H_v \eta_e} \tag{6}$$

where H_v is the lower heating value (J/g) of gasoline and η_e is the engine thermal efficiency.

The high-voltage battery pack consists of lithium-ion 18 650-type cells. The battery dynamics are governed by the following equations [35], [36]:

$$\begin{cases} P_b = V_{\text{oc}} I_b - I_b^2 R_{\text{in}} \\ \dot{\text{SoC}} = -\dfrac{I_b}{Q_b} = -\dfrac{V_{\text{oc}} - \sqrt{V_{\text{oc}}^2 - 4 R_{\text{in}} P_b}}{2 R_{\text{in}} Q_b} \end{cases} \tag{7}$$

where I_b and P_b are, respectively, the current (A) and the power (W) of the battery pack; R_{in} and V_{oc}, respectively, denote the internal resistance (Ω) and the open-circuit voltage (V), whose dynamic characteristics are shown in Fig. 2(b) (assuming that batteries operate at a constant temperature of 35 °C); and Q_b is the nominal capacity (A · s) of the battery pack. The battery SoC is subject to the constraints (SoC $\in$ [0.2, 0.8]), to ensure safe battery operation and prolong its service life [37]. According to the power balance, the battery power P_b is given by

$$P_b = \frac{\eta_m^{\kappa_m}}{r} T_d v_f - \eta_g T_e \omega_e - \frac{\kappa_c r_r \left(\eta_m^{\kappa_m} - \eta_g\right)}{r (r_r + r_s)} T_e v_f \tag{8}$$

where η_m and η_g represent the efficiency factors of the motor and the generator, respectively. The motor can either drive the wheels ($\kappa_m = -1$) or charge the battery by performing regenerative braking ($\kappa_m = 1$).

D. Energy Management Strategy

Charge depleting–charge sustaining (CD-CS) is a well-proved EMS [38], taking advantage of the PHEV's extended all-electric (or zero emissions) range and protecting battery cells from overcharge or overdischarge. Moreover, this strategy is favored by its simplicity and ease of implementation. According to the CD-CS model defined in our previously published study [39], the engine torque demand T_e is computed as a function of the engine speed ω_e and the battery SoC as follows:

$$T_e(\text{SoC}, \omega_e) = \begin{cases} 0, & \text{SoC} \in [\varepsilon_1, 1], \\ T_e^{\max}(\omega_e) \cdot \exp\left(-\dfrac{(\text{SoC} - \varepsilon_2)^2}{2\sigma^2}\right), & \text{SoC} \in [\varepsilon_2, \varepsilon_1], \\ T_e^{\max}(\omega_e), & \text{SoC} \in [0, \varepsilon_2], \end{cases} \tag{9}$$

where σ is a constant factor, ε_1 and ε_2 are two thresholds that are equal to 0.8 and 0.2, respectively, and $T_e^{\max}$ is the full-load torque of the engine, as shown in Fig. 2(a). The PHEV main specifications mentioned in this section are summarized in Table I.

TABLE I
MAIN SPECIFICATIONS OF THE POWER-SPLIT PHEV

Parameter	Value	Parameter	Value
m_0	1350 kg	r	0.28 m
A_f	2.2 m^2	ρ	1.225 kg/m^3
C_d	0.3	f	0.021
r_s	0.03 m	r_r	0.078 m
κ_c	3.9	Q_b	90000 A·s

III. Problem Formulation and Optimization Methods

Fig. 3 shows an overview of the multiobjective CACC and EMS co-optimization problem. The decision vector (or solution), the objective vector (or outcome), and the state vector are exemplified in subplots. Different driving cycles of the leading vehicle are provided for optimization and validation purposes. The formulated optimization problem is solved by the Pareto method or the weighted-sum method (serving as a benchmark), by guiding a population of candidate solutions toward better solutions that simultaneously minimize multiple objectives.

A. Multiobjective Problem Formulation

Fig. 3(c) shows that the decision vector $K = [k_v, k_s, \sigma]$ consists of the principal control parameters in CACC and EMS systems. k_v and k_s are gain factors in (2), which determine the car-following behavior; the variable σ in (9) governs the torque (or power) split. Previous studies [34], [39] have given the recommended value, $K_{\text{base}} = [0.58, 0.10, 0.10]$, which is utilized as the baseline scheme in this article.

As an image of the decision vector K through the optimization algorithm, the objective vector $J = [J_1, J_2, J_3]$ is mainly concerned with tracking safety, ride comfort, and energy efficiency as follows:

$$\begin{cases} \min\limits_K J_1 = \dfrac{1}{t_f} \displaystyle\int_0^{t_f} \|s(t) - s_{\text{des}}(t)\|_2 \, dt \\ \min\limits_K J_2 = \dfrac{1}{t_f} \displaystyle\int_0^{t_f} \|a_f(t)\|_2 \, dt \\ \min\limits_K J_3 = \dfrac{1}{1000\ t_f} \left(\displaystyle\int_0^{t_f} \dot{m}_f(t) H_v \, dt \right. \\ \qquad\qquad \left. + \left(\text{SoC}(t_f) - \text{SoC}(0)\right) Q_b V_b \right) \end{cases} \tag{10}$$

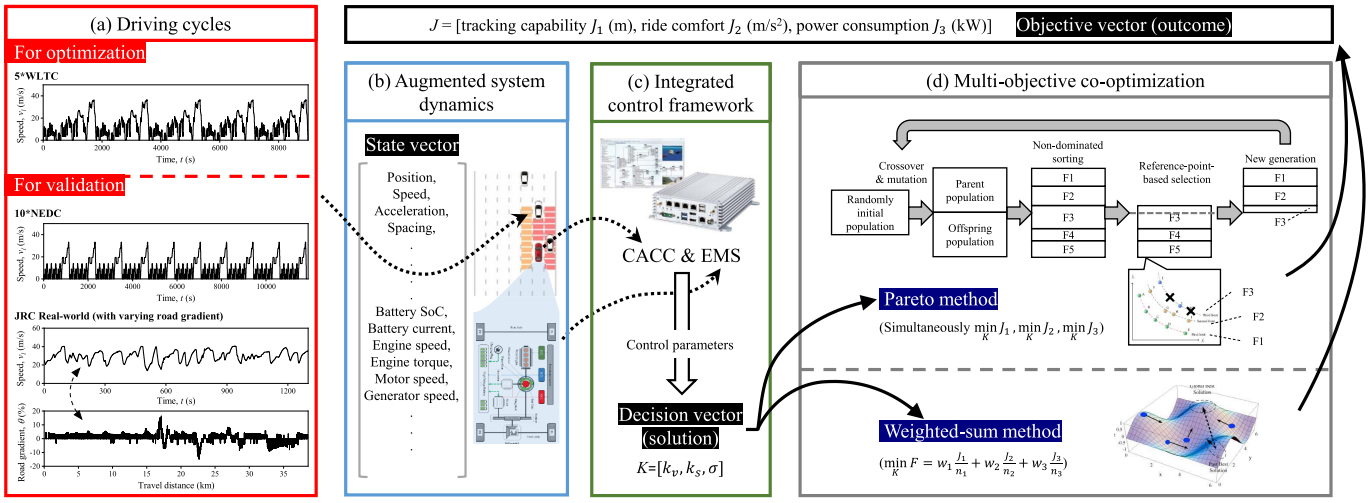

Fig. 3. Multiobjective co-optimization with the Pareto method and the weighted-sum method.

where t_f is the end time of the driving cycle adopted. Each element of the objective vector is defined as follows.

1) Tracking capability J_1 (m) is a two-norm function of tracking error [40] and an important indicator for improving car-following safety and traffic throughput [41].
2) Ride comfort J_2 (m/s^2) is defined as a two-norm function of the following vehicle's longitudinal acceleration. Although some studies utilize jerk as the indicator of ride comfort [24], acceleration is a more intuitive measure of the driver's sensation when driving on the road [32].
3) Power consumption J_3 (kW) is the average power demand to complete the driving cycle. The terms inside the parentheses represent the total energy consumption (J), including the consumed gasoline and the battery charge depletion [32].

Fig. 3(a) shows the lead vehicle's driving cycles: 1) 5*WLTC indicates five consecutive repetitions of the worldwide harmonized light vehicle test cycle; 2) 10*NEDC means ten consecutive repetitions of the new European driving cycle; 3) JRC Real-world, published by the European Commission–Joint Research Centre (JRC), is a highway driving trajectory with varying road gradient; this field test was conducted on a section of Autostrada A26 (Italy) between Ispra and Vicolungo, a 40-km trip, to collect driving data under actual traffic conditions. Among these driving cycles, the first one (5*WLTC) is applied in the multiobjective optimization process; the other two (10*NEDC and JRC Real-world) are utilized to validate the reliability and robustness of the resulting optimal solutions.

B. Multiobjective Optimization Methods

As shown in Fig. 3(d), the Pareto method and the weighted-sum method for solving the above-mentioned optimization problem are two evolutionary algorithms (EAs) generating high-quality solutions by relying on bioinspired operators, such as mutation, crossover, and selection. However, the two methods have different selection schemes, i.e., different approaches to ordering the objective vectors in each generation.

1) Pareto Method: For the formulated multiobjective CACC and EMS co-optimization problem, a single solution that simultaneously optimizes each objective is nonexistent. Instead, there exist a (possibly infinite) number of Pareto optimal solutions, in which one objective cannot be improved without degrading at least one of the other objectives. A solution K^1 is said to dominate (or Pareto) another solution K^2 (in notation, $K^1 \preceq K^2$) if the following conditions are met [31]:

$$\begin{cases} J_i(K^1) \le J_i(K^2), & \forall\ i \in [1,2,3] \\ J_j(K^1) < J_j(K^2), & \exists\ j \in [1,2,3]. \end{cases} \tag{11}$$

The solutions that are not dominated by others are called Pareto optimal K_{PF}. Their corresponding outcomes (or objective vectors J_{PF}) are represented by a PF. The high-level knowledge (e.g., tradeoffs and scale differences between the objectives) of the Pareto set (K_{PF}, J_{PF}) assists in finding a best compromise solution. To find an approximation of the entire PF, a nondominated sorting genetic algorithm (NSGA-III) [42], [43] is employed in this article.

2) Weighted-Sum Method: Serving as a benchmark, the weighted-sum method integrates different objectives into a single cost function using configurable weights. After the scalarization, the objective vectors can be ordered as per the composite cost value. Mathematically, the weighted-sum method can be represented by

$$\min_K F = \sum_{i=1}^{3} w_i \frac{J_i(K)}{n_i} \quad \text{for } w_i \ge 0 \text{ and } \sum_{i=1}^{3} w_i = 1 \tag{12}$$

where w_i is the weight factor and n_i is the normalization factor. Although this method is computationally efficient, the major limitation is that it cannot determine the factors w_i and n_i that can optimally balance and scale the objective functions for a problem with little or no information [31]. In this article, a particle swarm optimization (PSO) algorithm [5] is applied

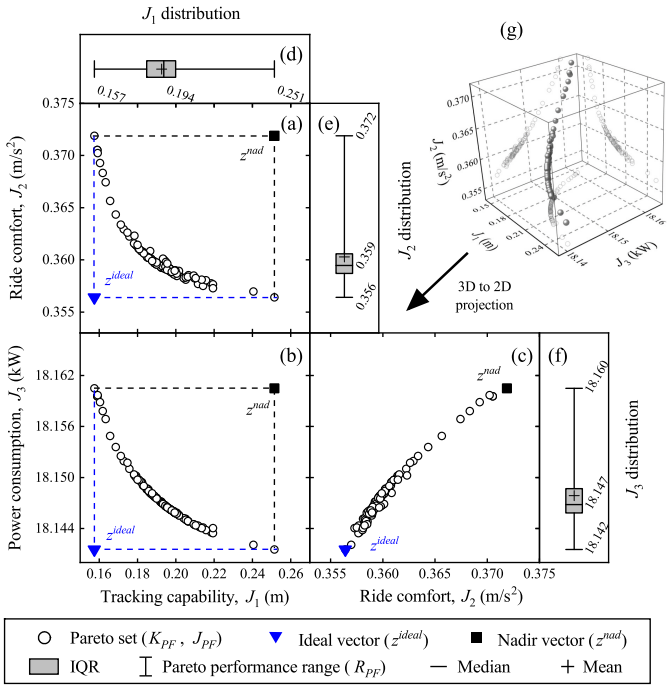

Fig. 4. Representative PF approximated by NSGA-III. (a) Projection onto the J_1 - J_2 plane. (b) Projection onto the J_1 - J_3 plane. (c) Projection onto the J_2 - J_3 plane. (d) Marginal distribution of J_1. (e) Marginal distribution of J_2. (f) Marginal distribution of J_3. (g) PF in 3D space.

to minimize the cost function F and find the corresponding optimal solution K_{WS}.

IV. Results and Discussion

This section will be divided into four parts. First, the PF (K_{PF}, J_{PF}) reveals the high-level knowledge, e.g., tradeoffs and scale differences between the objectives, for the CACC and EMS co-optimization problem. Second, the Pareto knowledge assists in finding a best compromise solution K^*_{PF}, whose safety and energy benefits are validated by comparing with the baseline scheme (K_{base}) in various driving conditions. Third, the weighted-sum optimal solutions with (K^P_{WS}) and without (K^B_{WS}) the Pareto knowledge highlight that the weighted-sum method cannot optimally scale the objective functions if the Pareto information is unknown. Finally, we compare the sensitivities of the objective functions to variations in the reaction time τ.

A. Pareto Frontier

Fig. 4 shows the representative PF approximated by NSGA-III. For visualization and analysis purposes, the 3-D objective vectors are projected onto the 2-D scatter plots of Fig. 4(a)–(c). The ideal (z^{ideal}) and the nadir (z^{nad}) vectors correspond to the lower and the upper boundaries, respectively. Fig. 4(a) shows a tradeoff between tracking capability J_1 and ride comfort J_2 since one of them will deteriorate when the other is improved on the PF. Fig. 4(b) shows a similar relationship between tracking capability J_1 and power consumption J_3. However, Fig. 4(c) shows a harmonious relationship between ride comfort J_2 and power consumption J_3 because the reduction of any one is rewarded with a simultaneous decrease in the other. It also suggests that the acceleration levels of the PHEV impact significantly on its energy consumption [41].

TABLE II
Marginal Distributions of Objectives on the PF

Objective	R_{PF}	Median
Tracking capability, J_1	0.094	0.194
Ride comfort, J_2	0.016	0.359
Power consumption, J_3	0.018	18.147

Marginal distributions of the objectives are illustrated by the box-whisker diagrams in Fig. 4(d)–(f). The height of the box is the interquartile range (IQR) between the first quartile (Q_1, 25%) and the third quartile (Q_3, 75%). The median (the band inside the box) denotes the second quartile (Q_2, 50%). The ends of the whisker represent the Pareto performance range ($R_{\mathrm{PF}} = z^{\mathrm{nad}} - z^{\mathrm{ideal}}$). Table II summarizes the R_{PF} values and the medians of the PF, indicating that different objective functions are measured on different scales. For example, the median of power consumption J_3 is two orders of magnitude larger than that of the tracking capability J_1.

B. Benefits of the Pareto Optimum

Usually, only one solution is required, but all Pareto solutions (K_{PF}) are considered equally good because their objective vectors J_{PF} cannot be ordered directly. To find a best compromise solution, a penalty function u utilizes the above high-level Pareto knowledge to rank the Pareto set [44]

$$\min_{K\in\mathrm{PF}} u(J(K)) = \min_{K\in\mathrm{PF}} \sum_{i=1}^{3} w_i \frac{J_i(K) - z_i^{\mathrm{ideal}}}{z_i^{\mathrm{nad}} - z_i^{\mathrm{ideal}}} \tag{13}$$

where z_i^{ideal} and z_i^{nad} adjust the objectives measured on different scales to a notionally common scale, and the weight factor w_i represents the decision maker's preferences, whose value is assigned as $w = [0.5, 0.25, 0.25]$ to balance the tradeoffs between the objectives. Consequently, the Pareto solution with the minimum penalty u is the best compromise one $K^*_{\mathrm{PF}} = [1.22, 1.06, 0.05]$ in this study and defined as the Pareto optimum.

Fig. 5 shows a comparison between the Pareto optimum (K^*_{PF}) and the baseline scheme (K_{base}) in terms of their car-following and power-split performances in the 5*WLTC driving test. Fig. 5(i) shows a zoomed portion of the inter-vehicle spacing s profiles of Fig. 5(a). It can be seen from these two graphs that K^*_{PF} can always meet the minimum spacing requirement in (3), namely, $s \geq 2.0$ m; this constraint, however, is violated by the K_{base} control design. Moreover, Fig. 5(b) shows that K^*_{PF} can significantly reduce tracking error $s - s_{\mathrm{des}}$, thus enhancing car-following safety. Fig. 5(c) and (d) shows the following vehicle's speed and acceleration, respectively. Fig. 5(e)–(h) compares the power-split dynamics of the two control schemes. For the K_{base} design, the engine and the generator started to work at ~1700 s, i.e., switching to the CS mode; the battery SoC was then kept at ~0.4. For the K^*_{PF} design, however, the CS mode was postponed until ~3000 s and the battery SoC was controlled at the lower level of ~0.3.

TABLE III
BENEFITS OF THE PARETO OPTIMUM K^*_{PF}

	5*WLTC			10*NEDC			JRC Real-world		
	J_1 (m)	J_2 (m/s^2)	J_3 (kW)	J_1 (m)	J_2 (m/s^2)	J_3 (kW)	J_1 (m)	J_2 (m/s^2)	J_3 (kW)
K_{base}	0.5640	0.3638	19.2638	0.3710	0.2588	12.9026	0.9462	0.4831	47.5019
K^*_{PF}	0.1858	0.3602	18.1484	0.0936	0.2634	11.7137	0.2939	0.4915	43.9082
Reduction (%)	67.06	0.99	5.79	74.77	-1.78	9.21	68.94	-1.74	7.57

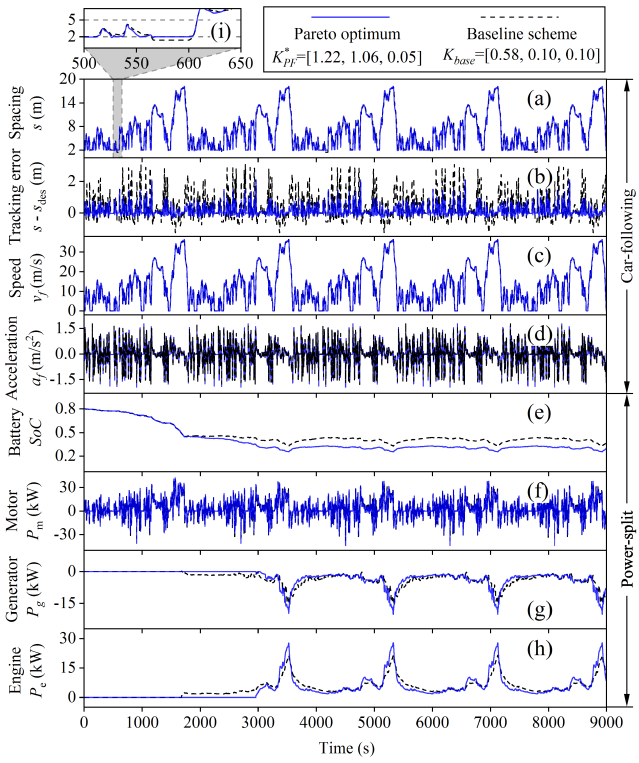

Fig. 5. Comparison of control performances between the Pareto optimum K^*_{PF} and the baseline scheme K_{base}. (a) Inter-vehicle spacing. (b) Tracking error. (c) Speed. (d) Acceleration. (e) Battery SoC. (f) Motor power. (g) Generator power. (h) Engine power.

Table III compares the control performances J_i between the Pareto optimum K^*_{PF} and the baseline scheme K_{base} in the optimization (5*WLTC) and validation (10*NEDC and JRC Real-world) driving cycles. The data highlight that the Pareto optimal solution for CACC and EMS design can provide considerable and consistent benefits in different driving conditions. For example, in the JRC Real-world driving cycle with varying road gradient, the Pareto optimum K^*_{PF} can reduce energy consumption (by 7.57%) and tracking error (by 68.94%) while simultaneously satisfying ride comfort needs.

C. Weighted-Sum Optimums

Serving as a benchmark, the weighted-sum method uses the same weight vector, $w = [0.5, 0.25, 0.25]$, as the Pareto method to balance the tradeoffs between the objectives. For comparison purposes, the weighted-sum method in this article utilizes two different normalization techniques [45] that are given in the following.

TABLE IV
COMPARISON OF THE PARETO AND THE WEIGHTED-SUM OPTIMUMS IN THE 5*WLTC DRIVING TEST

	K^*_{PF} [1.22, 1.06, 0.05]	K^P_{WS} [1.23, 1.06, 0.05]	K^B_{WS} [1.89, 2.49, 0.05]
J_1 (m)	0.1858	0.1864	0.1447
J_2 (m/s^2)	0.3602	0.3601	0.3758
J_3 (kW)	18.1484	18.1483	18.1976
Penalty u	30.2384	30.2640	50.0000

1) Normalization (without the Pareto knowledge) by objective values at the baseline point, $n = J(K_{\mathrm{base}})$. The corresponding weighted-sum optimum is (K^B_{WS}, J^B_{WS}).
2) Normalization (with the Pareto knowledge) by the Pareto performance range, $n = R_{\mathrm{PF}} = z^{\mathrm{nad}} - z^{\mathrm{ideal}}$. The corresponding weighted-sum optimum is (K^P_{WS}, J^P_{WS}).

Fig. 6(a)–(c) shows the evolutions of J^P_{WS} and J^B_{WS} during 30 PSO iterations. It is obvious that the weighted-sum method is computationally efficient because the objectives converged rapidly (within 20 generations). However, different normalization techniques lead to different final optimums. In Fig. 6(d)–(f), the weighted-sum optimums are projected onto 2-D planes and compared with the PF. It is worth noting that J^P_{WS} is located on the PF and very close to the Pareto optimum J^*_{PF}. On the contrary, J^B_{WS} presents an overoptimized tracking capability J_1, which can, in turn, compromise the other performance measures, i.e., the ride comfort J_2 and the power consumption J_3. Table IV summarizes the final optima through the Pareto method as well as the weighted-sum methods with differing normalization.

These comparisons reveal that the weighted-sum method cannot determine the normalization factors that can optimally scale the objective functions if the high-level Pareto knowledge is unknown before the optimization begins. The Pareto method can overcome this limitation by producing a set of Pareto optimal solutions. These solutions indicate tradeoffs and scale differences between the objectives and assist in finding a best compromise solution that can accurately capture the decision maker's preferences.

D. Sensitivities to the Reaction Time

Encompassing communication, sensing, and actuation delays, the reaction time τ in (2) and (4) is a major factor that impacts tracking safety, ride comfort, and fuel economy. This section demonstrates the sensitivities of the objectives to τ variations and compares the performance robustness of the Pareto and the weighted-sum optima.

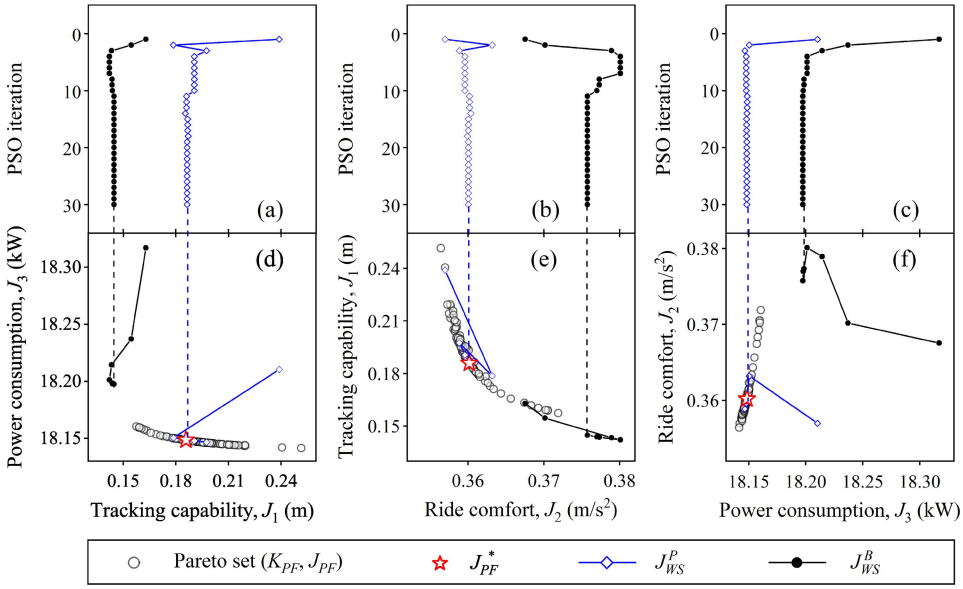

Fig. 6. Multiobjective optimization using weighted-sum methods. (a) PSO iteration of J_1. (b) PSO iteration of J_2. (c) PSO iteration of J_3. (d) Projection onto the J_1 - J_3 plane. (e) Projection onto the J_2 - J_1 plane. (f) Projection onto the J_3 - J_2 plane.

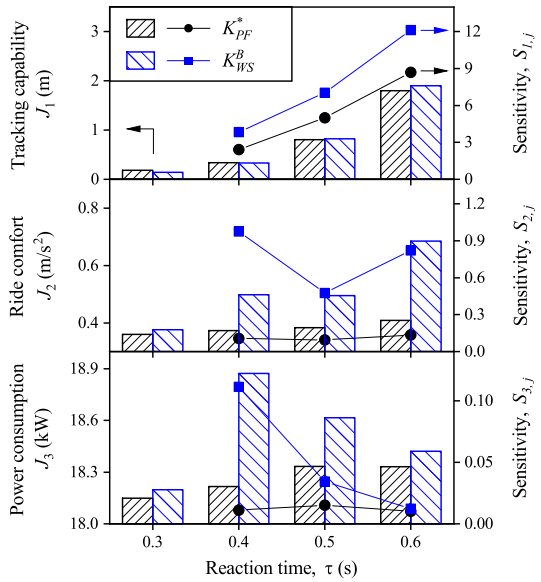

Fig. 7. Sensitivities of the objectives to reaction time τ variations.

The sensitivity of each objective to the reaction time variation can be calculated by [5]

$$S_{i,j} = \left| \frac{\big(J_i(\tau_j) - J_i(\tau_0)\big)/J_i(\tau_0)}{(\tau_j - \tau_0)/\tau_0} \right| \tag{14}$$

where $S_{i,j}$ is the sensitivity of the objective J_i $(i = 1, 2, 3)$ to the variation of the reaction time, $\tau_j \in [0.3, 0.4, 0.5, 0.6]$ s, and $J_i(\tau_0)$ is chosen as the reference corresponding to the situation when $\tau_j = \tau_0 = 0.3$ s. The larger the sensitivity value, the more significant the influence of reaction time on the outcome.

In Fig. 7, the tracking capability (J_1) shows the highest sensitivity to variation in τ. Its sensitivity $S_{1,j}$ increases with the increase in reaction time. The power consumption J_3 is the least sensitive criterion, whose sensitivity is two orders of magnitude smaller than that of J_1. Therefore, the reaction time impacts significantly on tracking safety, but its effect on energy saving is trivial. In addition, compared with the weighted-sum counterpart K^B_{WS}, the Pareto optimum K^*_{PF} always exhibits less sensitivity to τ variation for every objective, indicating a higher level of performance robustness against a range of operational delays in various driving scenarios.

V. Conclusion

In a vehicle control design, the co-optimization of electrification, automation, and connectivity is gaining traction among automakers and policymakers. Previous approaches, such as weighted-sum methods, overlook tradeoffs and scale differences inherent in these multiobjective problems, resulting in misleading optimizations. To overcome these limitations, this article proposes a Pareto-based framework demonstrated to optimize the system parameters of CACC and EMS for PHEVs. The high-level knowledge of the PF assists in finding a best compromise solution. The optimized systems can be directly applied in real applications. The results of this study are as follows.

1) The PF suggests that the comfort and the energy targets are harmonious, but they both conflict with the safety target. Their objective values are measured on different scales.
2) In the validation using real-world driving data, the Pareto optimum K^*_{PF} for CACC and EMS systems compared with the baseline scheme K_{base} can reduce energy consumption (by 7.57%) and tracking error (by 68.94%) while simultaneously satisfying ride comfort needs.
3) In contrast to the weighted-sum method, the proposed Pareto method can optimally balance and scale the multiple-objective functions and thus accurately capture the decision maker's preferences.

4) Sensitivity analysis proves that the vehicle reaction time impacts significantly on tracking safety, but its effect on energy saving is trivial.

ACKNOWLEDGMENT

This work was based on a collaboration agreement between the University of Birmingham and the European Commission–Joint Research Centre. The authors would like to thank B. Ciuffo for his support during this project.

REFERENCES

[1] M. A. Raposo *et al.*, *The Future of Road Transport—Implications of Automated, Connected, Low-Carbon and Shared Mobility*, Standard EUR 29748 EN, Publications Office of the European Union, Luxembourg, 2019. [Online]. Available: https://op.europa.eu/en/publication-detail/-/publication/c764dfe8-25fa-11ea-af81-01aa75ed71a1/language-en

[2] G. J. Offer, "Automated vehicles and electrification of transport," *Energy Environ. Sci.*, vol. 8, no. 1, pp. 26–30, Nov. 2014.

[3] L. Zhang, Y. Wang, and Z. Wang, "Robust lateral motion control for in-wheel-motor-drive electric vehicles with network induced delays," *IEEE Trans. Veh. Technol.*, vol. 68, no. 11, pp. 10585–10593, Nov. 2019.

[4] Y. Wang, Z. Wang, L. Zhang, M. Liu, and J. Zhu, "Lateral stability enhancement based on a novel sliding mode prediction control for a four-wheel-independently actuated electric vehicle," *IET Intell. Transp. Syst.*, vol. 13, no. 1, pp. 124–133, Jan. 2019.

[5] Q. Zhou, W. Zhang, S. Cash, O. Olatunbosun, H. Xu, and G. Lu, "Intelligent sizing of a series hybrid electric power-train system based on chaos-enhanced accelerated particle swarm optimization," *Appl. Energy*, vol. 189, pp. 588–601, Mar. 2017.

[6] Q. Zhou *et al.*, "Multi-step reinforcement learning for model-free predictive energy management of an electrified off-highway vehicle," *Appl. Energy*, vol. 255, Dec. 2019, Art. no. 113755.

[7] J. Li, Q. Zhou, H. Williams, and H. Xu, "AC-back competitive learning mechanism for fuzzy logic based supervisory control system of hybrid electric vehicles," *IEEE Trans. Ind. Electron.*, to be published.

[8] J. Li *et al.*, "Dual-loop online intelligent programming for driver-oriented predict energy management of plug-in hybrid electric vehicles," *Appl. Energy*, vol. 253, Nov. 2019, Art. no. 113617.

[9] M. Makridis, K. Mattas, and B. Ciuffo, "Response time and time headway of an adaptive cruise control. An empirical characterization and potential impacts on road capacity," *IEEE Trans. Intell. Transp. Syst.*, to be published.

[10] B. Ciuffo, M. Makridis, T. Toledo, and G. Fontaras, "Capability of current car-following models to reproduce vehicle free-flow acceleration dynamics," *IEEE Trans. Intell. Transp. Syst.*, vol. 19, no. 11, pp. 3594–3603, Nov. 2018.

[11] V. Milanés and S. E. Shladover, "Modeling cooperative and autonomous adaptive cruise control dynamic responses using experimental data," *Transp. Res. C, Emerg. Technol.*, vol. 48, pp. 285–300, Nov. 2014.

[12] L. Guo, H. Chen, Q. Liu, and B. Gao, "A computationally efficient and hierarchical control strategy for velocity optimization of on-road vehicles," *IEEE Trans. Syst., Man, Cybern. Syst.*, vol. 49, no. 1, pp. 31–41, 1st Quart., 2018.

[13] C. M. Martinez, X. Hu, D. Cao, E. Velenis, B. Gao, and M. Wellers, "Energy management in plug-in hybrid electric vehicles: Recent progress and a connected vehicles perspective," *IEEE Trans. Veh. Technol.*, vol. 66, no. 6, pp. 4534–4549, Jun. 2017.

[14] F. Zhang, X. Hu, R. Langari, and D. Cao, "Energy management strategies of connected HEVs and PHEVs: Recent progress and outlook," *Progr. Energy Combustion Sci.*, vol. 73, pp. 235–256, Jul. 2019.

[15] D. Maamria, K. Gillet, G. Colin, Y. Chamaillard, and C. Nouillant, "Computation of eco-driving cycles for hybrid electric vehicles: Comparative analysis," *Control Eng. Pract.*, vol. 71, pp. 44–52, Feb. 2018.

[16] G. Heppeler, M. Sonntag, U. Wohlhaupter, and O. Sawodny, "Predictive planning of optimal velocity and state of charge trajectories for hybrid electric vehicles," *Control Eng. Pract.*, vol. 61, pp. 229–243, Apr. 2017.

[17] L. Guo, B. Gao, Y. Gao, and H. Chen, "Optimal energy management for HEVs in eco-driving applications using bi-level MPC," *IEEE Trans. Intell. Transp. Syst.*, vol. 18, no. 8, pp. 2153–2162, Aug. 2017.

[18] J. Hu, Y. Shao, Z. Sun, M. Wang, J. Bared, and P. Huang, "Integrated optimal eco-driving on rolling terrain for hybrid electric vehicle with vehicle-infrastructure communication," *Transp. Res. C, Emerg. Technol.*, vol. 68, pp. 228–244, Jul. 2016.

[19] A. Plianos, T. Jokela, and M. Hancock, "Predictive energy optimization for connected and automated HEVs," Jaguar Land Rover, Coventry, U.K., SAE Tech. Paper 2018-01-1179, 2018.

[20] G. Li and D. Gorges, "Ecological adaptive cruise control and energy management strategy for hybrid electric vehicles based on heuristic dynamic programming," *IEEE Trans. Intell. Transp. Syst.*, vol. 20, no. 9, pp. 3526–3535, Sep. 2019.

[21] M. Vajedi and N. L. Azad, "Ecological adaptive cruise controller for plug-in hybrid electric vehicles using nonlinear model predictive control," *IEEE Trans. Intell. Transp. Syst.*, vol. 17, no. 1, pp. 113–122, Jan. 2016.

[22] B. Sakhdari, M. Vajedi, and N. L. Azad, "Ecological adaptive cruise control of a plug-in hybrid electric vehicle for urban driving," in *Proc. IEEE 19th Int. Conf. Intell. Transp. Syst. (ITSC)*, Nov. 2016, pp. 1739–1744.

[23] S. Xie, X. Hu, T. Liu, S. Qi, K. Lang, and H. Li, "Predictive vehicle-following power management for plug-in hybrid electric vehicles," *Energy*, vol. 166, pp. 701–714, Jan. 2019.

[24] L. Li, X. Wang, and J. Song, "Fuel consumption optimization for smart hybrid electric vehicle during a car-following process," *Mech. Syst. Signal Process.*, vol. 87, pp. 17–29, Mar. 2017.

[25] S. Qiu, L. Qiu, L. Qian, and P. Pisu, "Hierarchical energy management control strategies for connected hybrid electric vehicles considering efficiencies feedback," *Simul. Model. Pract. Theory*, vol. 90, pp. 1–15, Jan. 2019.

[26] M. Ghasemi and X. Song, "Powertrain energy management for autonomous hybrid electric vehicles with flexible driveline power demand," *IEEE Trans. Control Syst. Technol.*, vol. 27, no. 5, pp. 2229–2236, Sep. 2019.

[27] G. Ma, M. Ghasemi, and X. Song, "Integrated powertrain energy management and vehicle coordination for multiple connected hybrid electric vehicles," *IEEE Trans. Veh. Technol.*, vol. 67, no. 4, pp. 2893–2899, Apr. 2018.

[28] M. Hovgard, O. Jonsson, N. Murgovski, M. Sanfridson, and J. Fredriksson, "Cooperative energy management of electrified vehicles on hilly roads," *Control Eng. Pract.*, vol. 73, pp. 66–78, Apr. 2018.

[29] B. Chen, S. A. Evangelou, and R. Lot, "Series hybrid electric vehicle simultaneous energy management and driving speed optimization," *IEEE/ASME Trans. Mechatronics*, vol. 24, no. 6, pp. 2756–2767, Dec. 2019.

[30] J. Borek, B. Groelke, C. Earnhardt, and C. Vermillion, "Economic optimal control for minimizing fuel consumption of heavy-duty trucks in a highway environment," *IEEE Trans. Control Syst. Technol.*, pp. 1–13, 2019.

[31] M. Awad and R. Khanna, "Multiobjective optimization," in *Efficient Learning Machines*. Berkeley, CA, USA: Springer, 2015, pp. 185–208.

[32] Y. Luo, T. Chen, S. Zhang, and K. Li, "Intelligent hybrid electric vehicle ACC with coordinated control of tracking ability, fuel economy, and ride comfort," *IEEE Trans. Intell. Transp. Syst.*, vol. 16, no. 4, pp. 2303–2308, Aug. 2015.

[33] B. van Arem, C. J. G. van Driel, and R. Visser, "The impact of cooperative adaptive cruise control on traffic-flow characteristics," *IEEE Trans. Intell. Transp. Syst.*, vol. 7, no. 4, pp. 429–436, Dec. 2006.

[34] H. S. Mahmassani, "50th anniversary invited article—Autonomous vehicles and connected vehicle systems: Flow and operations considerations," *Transp. Sci.*, vol. 50, no. 4, pp. 1140–1162, 2016.

[35] T. Liu, X. Hu, S. E. Li, and D. Cao, "Reinforcement learning optimized look-ahead energy management of a parallel hybrid electric vehicle," *IEEE/ASME Trans. Mechatronics*, vol. 22, no. 4, pp. 1497–1507, Aug. 2017.

[36] K. Wu, M. Kuang, M. Milacic, X. Zhang, and J. Sun, "Analysis of effects of fuel cell system dynamics on optimal energy management," in *Proc. ASME Dyn. Syst. Control Conf.* New York, NY, USA: American Society of Mechanical Engineers, 2017, pp. 1–10

[37] X. Hu, C. M. Martinez, and Y. Yang, "Charging, power management, and battery degradation mitigation in plug-in hybrid electric vehicles: A unified cost-optimal approach," *Mech. Syst. Signal Process.*, vol. 87, pp. 4–16, Mar. 2017.

[38] Z. Chen, R. Xiong, C. Wang, and J. Cao, "An on-line predictive energy management strategy for plug-in hybrid electric vehicles to counter the uncertain prediction of the driving cycle," *Appl. Energy*, vol. 185, pp. 1663–1672, Jan. 2017.

[39] Q. Zhou, Y. Zhang, Z. Li, J. Li, H. Xu, and O. Olatunbosun, "Cyber-physical energy-saving control for hybrid aircraft-towing tractor based on online swarm intelligent programming," *IEEE Trans Ind. Informat.*, vol. 14, no. 9, pp. 4149–4158, Dec. 2017.
[40] D. Corona, M. Lazar, B. De Schutter, and M. Heemels, "A hybrid MPC approach to the design of a smart adaptive cruise controller," in *Proc. IEEE Int. Symp. Intell. Control*, Oct. 2006, pp. 231–236.
[41] S. Li, K. Li, R. Rajamani, and J. Wang, "Model predictive multi-objective vehicular adaptive cruise control," *IEEE Trans. Control Syst. Technol.*, vol. 19, no. 3, pp. 556–566, May 2011.
[42] K. Deb and H. Jain, "An evolutionary many-objective optimization algorithm using reference-point-based nondominated sorting approach, part I: Solving problems with box constraints," *IEEE Trans. Evol. Comput.*, vol. 18, no. 4, pp. 577–601, Aug. 2014.
[43] H. Jain and K. Deb, "An evolutionary many-objective optimization algorithm using reference-point based nondominated sorting approach, part II: Handling constraints and extending to an adaptive approach," *IEEE Trans. Evol. Comput.*, vol. 18, no. 4, pp. 602–622, Aug. 2014.
[44] S. H. R. Pasandideh and S. T. A. Niaki, "Multi-response simulation optimization using genetic algorithm within desirability function framework," *Appl. Math. Comput.*, vol. 175, no. 1, pp. 366–382, Apr. 2006.
[45] Z. Chen and S. Andresen, "A multiobjective optimization model of production-sourcing for sustainable supply chain with consideration of social, environmental, and economic factors," *Math. Problems Eng.*, vol. 2014, pp. 1–11, 2014.

Yinglong He received the B.Eng. and M.Res. degrees in energy and power engineering from the Huazhong University of Science and Technology, Wuhan, China, in 2014 and 2017, respectively. He is currently pursuing the Ph.D. degree with the Intelligent Vehicle Control Team, University of Birmingham, Birmingham, U.K., through the scholarship.

His current research interests include intelligent transportation, vehicle dynamics, driver behavior, multiobjective optimization, and machine learning.

Quan Zhou received the B.Eng. and M.Res. degrees (Hons.) in vehicle engineering from the Wuhan University of Technology, Wuhan, China, in 2012 and 2015, respectively.

He is currently a Research Fellow with the Intelligent Vehicle Control Team, Vehicle and Engine Technology Research Centre, University of Birmingham, Birmingham, U.K. His research interests include vehicle system modeling, hybrid electric vehicle (HEV)/EV design optimization, optimal control, and artificial intelligence for future HEVs and connected and autonomous vehicles (CAVs).

Michail Makridis received the Ph.D. degree in image processing and machine intelligence from the Democritus University of Thrace, Xanthi, Greece, in 2010.

Since 2012, he has been a Researcher and a Science and Policy Officer with the European Commission–Joint Research Centre, Ispra, Italy. He is the author of various publications in the fields of traffic modeling and simulation, image processing, and machine learning. His research interests are in intelligent transportation systems, simulation of vehicle dynamics and driver behavior, energy demand and emissions, image segmentation and classification, natural language processing, and sequential pattern mining.

Dr. Makridis is currently a reviewer for international journals.

Konstantinos Mattas received the B.Eng. degree in civil engineering (specialized in transportation) and the M.Sc. degree in applied mathematics, from the Democritus University of Thrace, Xanthi, Greece, in 2014 and 2017, respectively, where he is currently pursuing the Ph.D. degree with a focus on fuzzy logic applications in transportation engineering.

Since 2017, he has been working with the European Commission–Joint Research Centre, Ispra, Italy. His research interests are in intelligent transportation systems, simulation of vehicle dynamics and driver behavior, microscopic simulation of traffic networks and network control, optimization, and traffic safety.

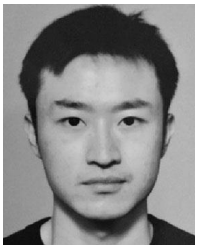

Ji Li received the B.Eng. degree in engineering from the Chongqing University of Technology, Chongqing, China, in 2015. He is currently pursuing the Ph.D. degree with the Intelligent Vehicle System and Control Team, University of Birmingham, Birmingham, U.K.

His current research interests include fuzzy mathematics, deep reinforcement learning, transfer learning, and development of driving behavior recognition, human–machine interaction, and vehicle systems optimization.

Huw Williams received the bachelor's degree in mathematics from the University of Oxford, Oxford, U.K., in 1978, and the Ph.D. degree in theoretical mechanics from the University of East Anglia, Norwich, U.K., in 1983.

He is currently an Honorary Professor in automotive engineering with the University of Birmingham, Birmingham, U.K. He has over 20 years' experience in the automotive industry. He joined Jaguar Land Rover, Coventry, U.K., in 1986, where he worked in research and development by applying mathematical modeling techniques to all aspects of vehicle technology.

Dr. Williams is a Chartered Fellow of the Institute of Mathematics and its Applications and a fellow of the Royal Statistical Society.

Hongming Xu received the Ph.D. degree in mechanical engineering from Imperial College London, London, U.K., in 1995.

He is currently a Professor of energy and automotive engineering with the University of Birmingham, Birmingham, U.K., where he is also the Head of the Vehicle and Engine Technology Research Centre. He has six years of industrial experience with Jaguar Land Rover, Coventry, U.K., and Premier Automotive Group of Ford, U.K. He has authored or coauthored more than 300 journal and SAE technical publications on advanced vehicle powertrain systems involving both experimental and modeling studies.

Dr. Xu is a fellow of SAE International and IMechE.